frontiers in Materials

ORIGINAL RESEARCH
published: 16 June 2021
doi: 10.3389/fmats.2021.680776

Enhanced Mechanical Properties of Fe-Mn-Al-C Low Density Steel *via* Aging Treatment

*Li Kang[1], Hao Yuan[2], Hua-ying Li[1], Ya-feng Ji[2], Hai-tao liu[3] and Guang-ming Liu[1]**

[1]School of Materials Science and Engineering, Taiyuan University of Science and Technology, Taiyuan, China, [2]School of Mechanical Engineering, Taiyuan University of Science and Technology, Taiyuan, China, [3]State Key Laboratory of Rolling and Automation, Northeastern University, Shenyang, China

This study investigated the tensile properties and deformation behavior of an aged Fe-26Mn-6Al-1C (mass%) alloy with a stacking fault energy of approximately 60 mJ·m^{-2}. The results show that an ordered phase with a "short-range ordering" (SRO) structure formed after aging at 550°C for 10 h, further increasing the aging time to 48 h. Lamellar second-phase precipitates appeared at the austenitic grain boundaries. The aged sample at 550°C for 10 h exhibited an enhanced tensile strength (~898 MPa) without notably sacrificing uniform elongation (~46.3%), which was mainly attributed to the relatively high strain hardening in the entire plastic deformation due to the synergistic effects of planar slip, twinning-induced plasticity (TWIP), microband-induced plasticity (MBIP), and especially the formation of short-range ordering.

Keywords: Fe-Mn-Al-C alloy, age-precipitated particles, short range ordering, deformation twinning, strain hardening rate

OPEN ACCESS

Edited by:
Peter Hodgson,
Deakin University, Australia

Reviewed by:
Zhiqiang Wu,
Hunan University of Science and Technology, China
Pavlo Maruschak,
Ternopil Ivan Pului National Technical University, Ukraine

****Correspondence:***
Guang-ming Liu
brightliu2008@126.com

Specialty section:
This article was submitted to Structural Materials, a section of the journal Frontiers in Materials

Received: *15 March 2021*
Accepted: *24 May 2021*
Published: *16 June 2021*

Citation:
Kang L, Yuan H, Li H, Ji Y, liu H and Liu G (2021) Enhanced Mechanical Properties of Fe-Mn-Al-C Low Density Steel via Aging Treatment. Front. Mater. 8:680776. doi: 10.3389/fmats.2021.680776

INTRODUCTION

Fe-Mn-Al-C steels have been extensively researched over the past several decades due to the high specific strength and stiffness of this material, which is a good trade-off between high ultimate tensile strength and good tensile ductility (Frommeyer and Brüx, 2006; Li et al., 2015; Klimova et al., 2017; Sarkar et al., 2019; Choi et al., 2020; Li et al., 2020) when compared with conventional high strength steels. The composition of the light high-Mn steel is mainly based on the traditional high-Mn steel composition, by increasing the content of carbon and manganese and adding a certain amount of aluminum. As a main alloying element, Mn has the function of enlarging the austenite region and stabilizing the austenite structure. The addition of Al to high Mn austenitic steels not only reduces the weight of the automotive body due to its lower density but also varies the deformation mechanisms of steels from either transformation-induced plasticity (TRIP) or twinning-induced plasticity (TWIP) (Grässel et al., 2000; Sohn et al., 2014; Yuan et al., 2015; Huang et al., 2017; Luo and Huang, 2018) to dislocation slip due to the increased stacking fault energy (SFE) (Frommeyer and Brüx, 2006; Li et al., 2015; Choi et al., 2020; Li et al., 2020). Microband-induced plasticity (MBIP) was also discovered by Frommeyer and Brux (Frommeyer and Brüx, 2006) in high Mn-Al austenitic alloys with the relatively high SFE value of 110 mJ·m^{-2} suppressing the formation of martensitic or severe mechanical twinning.

There has been dramatically growing interest in high Mn-Al austenite alloys containing carbon due to the presence of κ-carbide ($(Fe,Mn)_3AlC$) particles (James, 1969; Kayak, 1969; Choo and Han, 1985; Han et al., 1986; Ishida et al., 1990; Choo et al., 1997; Frommeyer and Brüx, 2006; Choi et al., 2020; Li et al., 2020). In the late 1970s, the $(Fe,Mn)_3A1C$ κ-carbide precipitates with an ordered L'l2

crystal structure were first observed in high Al and C Fe-Mn-Al-C alloys by James (1969); Kayak (1969); Ishida et al, (1990) established the relationship between different α, γ and κ phases based on the phase constitutions of Fe-(20-30)Mn-Al-C alloys. Choo et al. (Choo and Han, 1985; Han et al., 1986) described the κ-carbides with a face-center cubic (fcc) based phase with an ordered L'l2 structure, which was similar to that of Ll2. Frommeyer and Brux Choi (Frommeyer and Brüx, 2006) reported that the nanosized κ-carbides with a perovskite structure in a Fe-28Mn-10Al-0.5C alloy were accompanied by shear bands, which was also verified by Choi et al., (2010). Accordingly, the tensile ductility was enhanced by the nanosized (Fe,Mn)3AlC κ-carbide precipitates in the austenitic Fe-Mn-Al-C alloys (Frommeyer and Brüx, 2006; Choi et al., 2020; Li et al., 2020) due to the so-called MBIP effect, which was comparable to the loss of ductility resulting from the unfavorable morphology of κ-carbides in ferrite or ferrite-austenite duplex lightweight Fe-Mn-Al-C steels.

The better strengthening effect of high-Mn steel could be obtained by examining the composite treatment of aging and deformation, which not only improves the ductility but also the strength of the steel. The stress flow behavior of alloys with various hot forming conditions greatly affects the evolution of their microstructure (Fang et al., 2016). At present, the discussion on the microstructure evolution of hign-Mn Fe-Mn-Al-C steels via aging treatment is still ongoing, and the influence of microstructure on the deformation mechanism also needs to be further studied, for optimizing the properties of the experimental steel.

In the present study, a lightweight Fe-26Mn-6Al-1.0C (mass, %) austenitic alloy with a stacking fault energy (SFE) value of approximately 60 $mJ{\cdot}m^{-2}$ was used to investigate the formation of a new strengthening phase with a "short-range ordering" (SRO) structure. The present study also clarifies the influence of aging temperature and time on microstructural evolution, tensile properties, and deformation behavior of Fe-26Mn-6Al-1.0C.

EXPERIMENTAL PROCEDURES

A Fe-26Mn-5.84Al-1.0C (mass, %) alloy was designed. Its SFE value was estimated to be approximately 60 $mJ{\cdot}m^{-2}$ based on the thermodynamic models reported by several researchers (Grassel et al., 1997; Dumay et al., 2008; Song et al., 2017). The alloy was prepared in an induction furnace by induction melting and then cast into small rectangular ingots. The ingots were homogenized at 1,200°C for 2 h and hot-rolled at around 1,050°C to 3 mm in thickness with a total reduction of 85%.

Tensile specimens, whose gauge width and length are 10 and 40 mm, respectively, were taken from the hot-rolled strip with the tensile axis parallel to the rolling direction. The tensile specimens were solution-treated at 1,100°C for 1 h, followed by water quenching to room temperature. Meanwhile, the solution-treated tensile specimens were further aged at temperatures ranging from 450 to 550°C for 10 h to study the precipitation behavior of experimental steel. Uniaxial tensile tests were carried out on an Instron 5,967 30 kN machine at an initial strain rate of $1 \times 10^{-3}\ s^{-1}$.

The microstructural characterization was performed using an optimal microscope (OM, Olympus DSX500) and transmission electron microscope (TEM, Tecnai $G^2$20) operated at 200 kV. TEM specimens were prepared as thin foils by mechanical grinding and twin-jet electropolishing in a mixture of 8% perchloric acid and 90% alcohol at −35°C with an applied potential of 50 V. The phase constituents were determined by an X-ray diffractometer (XRD, D/Max-Ra) with CuK_α radiation in the range of 40 to 120°.

RESULTS AND DISCUSSIONS

The hot-rolled Fe-26Mn-5.84Al-1.0C alloy shows a single fcc-structured γ phase with an average grain size of about 20 μm, together with dislocation tangle, stacking fault, and annealing twins. After solution treatment at 1,100°C for 1 h, the grain size of γ was measured at around 130 μm with some amount of annealing twins (**Figure 1A**), and only γ phase peaks were detected by XRD patterns (**Figure 2**). In addition, there existed a relatively large number of dislocations in the solution-treated alloy (**Figure 3A**). These dislocations were periodically arranged in a plane, as schematically illustrated in **Figure 3B**.

After aging treatment at temperatures ranging from 450 to 550°C for 10 h, the optical micrographs (**Figures 1B–D**) appeared no significant change, when compared with that of the solution-treated sample (**Figure 1A**). The intensities of both (200)γ and (220)γ peaks increased with increasing aging temperature, while that of (111)γ decreased, as shown in **Figure 2**. It should be noted that no second-phase particles could be observed by TEM under all experimental conditions. It has been reported that the coarse second-phase particles could be observed along the austenitic grain boundaries by optical microscopy for the Fe-(28–31.5)Mn-(8.0–9.0)Al-(0.8–1.05)C alloys aged for 120–129 h (Hwang et al., 1993), which was different from the present short-time aged Fe-26Mn-5.84Al-1.0C alloy.

Table 1 shows the tensile properties of the solution-treated Fe-26Mn-5.84Al-1.0C alloy, in conjunction with the aged samples at 450–550°C for 10 h. As a whole, the austenitic Fe-26Mn-5.84Al-1.0C alloy exhibited yield strength (YS) of 378–480 MPa, UTS of 727–898 MPa, and total elongation (δ) of 47–53.2%. The values of UTS × δ ranged from 36.0 to 45.0 GPa·% for the present alloys, which were smaller than those (67.7–84.6 GPa·%) of the Fe-28Mn-9Al-0.8C alloy fabricated by cold rolling and heating treatment studied by Yoo et al. (Choi et al., 2020). This difference was likely associated with the larger size of austenitic grains, ~130 μm for the present alloys, while that was only 5–38 μm for the Fe-28Mn-9Al-0.8C alloy (Choi et al., 2020). It was worth noting that the aged Fe-26Mn-5.84Al-1.0C alloy at 550°C for 10 h exhibited an extremely high UTS value with no loss of ductility, compared with the other solution-treated or aged samples in this study (Kayak et al., 1969; Kalashnikov et al., 2000). To investigate the reason for the enhanced ultimate tensile strength and ductility, the precipitation

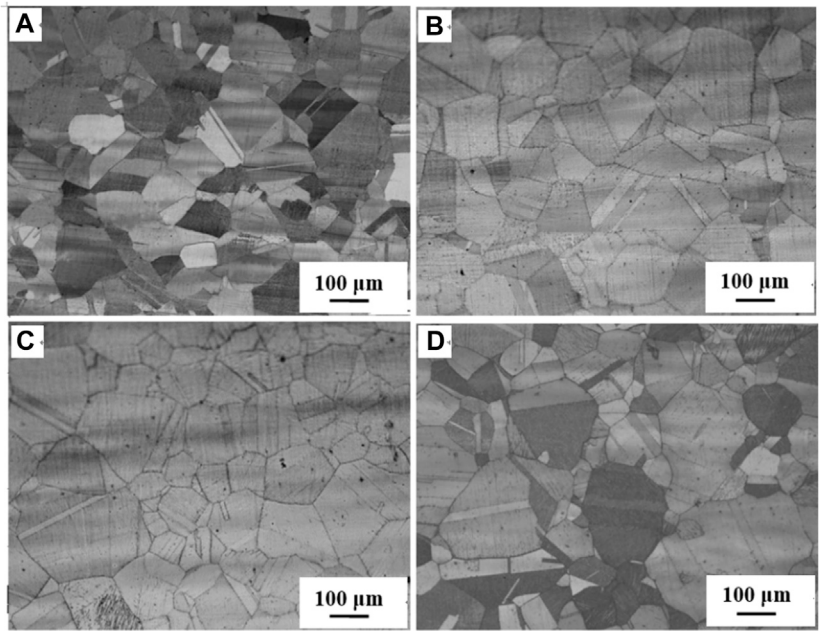

FIGURE 1 | Optical micrographs of the Fe-26Mn-5.84Al-1.0C alloy subjected to **(A)** solution treatment at 1,100°C for 1 h and ageing treatment for 10 h at three different temperatures: 450 °C **(B)**, 500°C **(C)** and 550°C **(D)**.

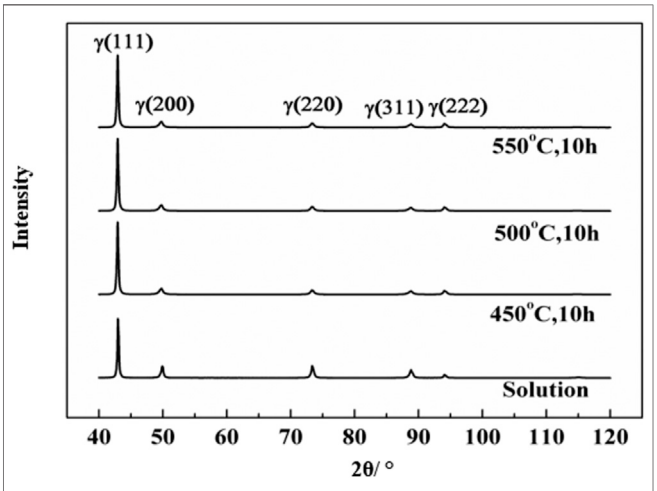

FIGURE 2 | XRD patterns of the Fe-26Mn-5.84Al-1.0C alloy subjected to solution treatment at 1,100°C for 1 h and aging treatment at 450, 500, and 550°C for 10 h.

behavior during aging treatment was clarified, together with further analysis of deformation mechanisms during tensile tests.

Figure 4 reveals the true stress (σ) and strain hardening rate (dσ/dε) with respect to true strain (ε) in the solution-treated Fe-26Mn-5.84Al-1.0C alloy, in conjunction with the aged samples at 450, 500 and 550°C for 10 h. All tensile samples exhibited continuous yielding and extensive strain hardening behaviors, which was similar to the conventional high Mn austenitic steels (Yuan et al., 2015; Huang et al., 2017). In the entire plastic deformation region, the aged Fe-26Mn-5.84Al-1.0C samples exhibited the three-stage strain-hardening behavior, regardless of aging temperature. The dσ/dε value rapidly decreased at stage I, remained a constant at stage II, and then decreased again at stage III as the true strain increased. The significant difference between the solution-treated and aged samples was that the dσ/dε value of the former gradually decreased with ε at stage II; whereas the aged sample at 550°C for 10 h showed the relatively higher strain hardening capability during the whole plastic deformation. According to the true strain value (ε) when the peak value of dσ/dε appeared, the plastic instability had been delayed after aging. This could be responsible for high UTS with no loss of ductility in the aged Fe-26Mn-5.84Al-1.0C alloy at 550°C for 10 h.

To support the dominant deformation mechanisms of an aged Fe-26Mn-6Al-1C alloy at 550 °C for 10 h, the representative TEM morphologies were supplemented. As displayed in **Figure 1D**, the initial microstructure prior to tensile testing was the coarse austenite grains and annealing twins. As the tensile strain was about 5%, microbands were observed, implying the dominant deformation mode was MB at the early stage of plastic deformation. Upon further straining, the dislocations made equal spacing arrays along the two principal directions and the dislocation densities increased without altering the slip directions (Ding et al., 2013). After a tensile fracture, the well-developed microbands and deformation twins (**Figure 5B**) became dominant, indicating that both TWIP and MBIP effects occurred in the aged Fe-26Mn-5.84Al-1.0C alloy with a relatively high SFE value of 60 $mJ \cdot m^{-2}$. The formation of microbands and deformation twins would give rise to a remarkable difference in strain hardening phenomena as both of them acted as effective obstacles to dislocation glide (Urrutia and Raabe, 2011; Ding et al., 2013). In contrast, only a large number of microbands were observed in the solution-treated

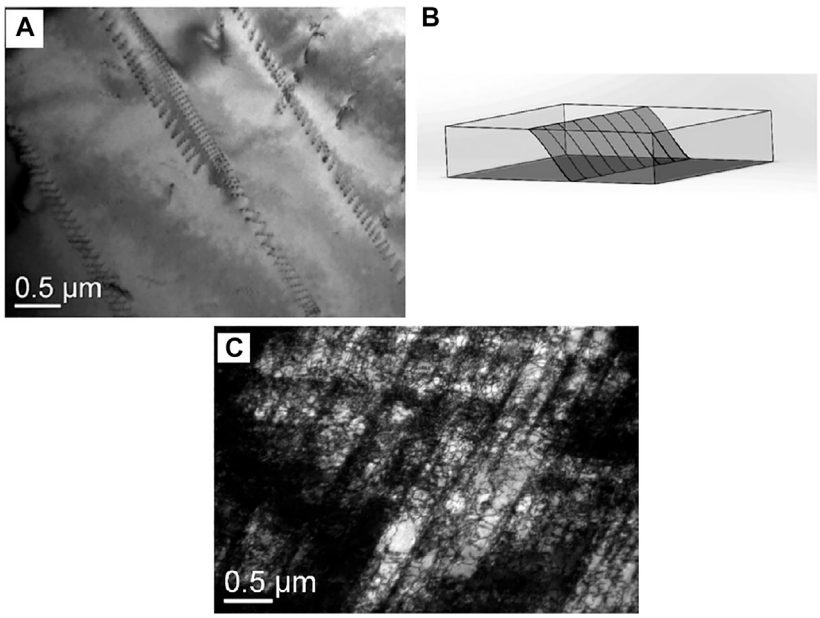

FIGURE 3 | Dislocation alignment in planar **(A)** and the corresponding schematic diagram of Fe-26Mn-5.84Al-1.0C alloy at 1,100°C for 1 h **(B)**. **(C)** shows the micro-bands after interrupted tensile deformation up to 30%.

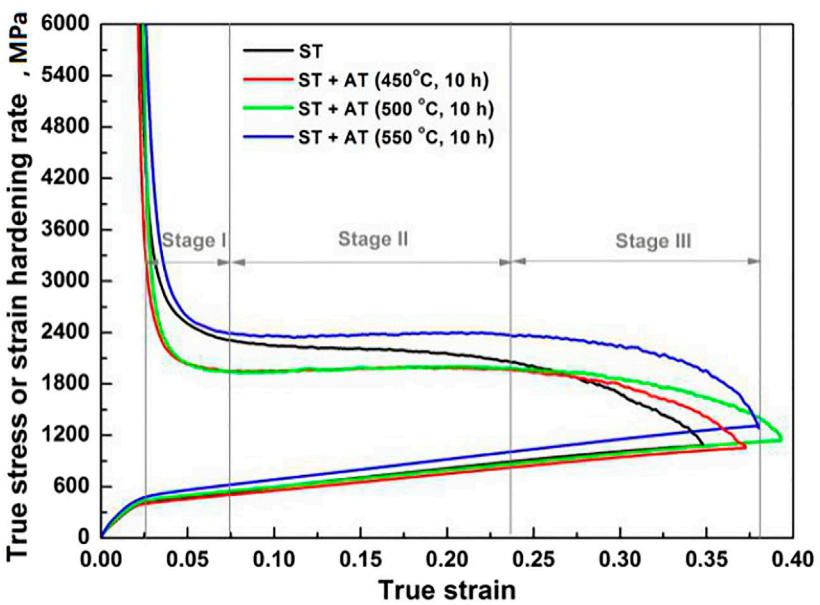

FIGURE 4 | Changes in true stress (σ) and strain hardening rate (dσ/d *& epsi*) with true strain (*& epsi*) in the solution-treated Fe-26Mn-5.84Al-1.0C alloy, along with the aged samples at 450, 500, and 550°C for 10 h.

sample (**Figure 3C**), implying that MBIP was a dominant deformation mechanism.

An island-like phase within the γ matrix was found (**Figure 5C**), which was also called an ordered phase with a "short-range ordering" (SRO) structure, as verified by the SAD pattern (see an inset at the upper right of **Figure 5C**). It was also revealed that the SRO phase exhibited a coherent orientation relationship with γ matrix [100] SRO/[100]γ, which was similar to that of SRO in $AuCu_3$ superalloys (Hiraga et al., 1982). In the preliminary work, Choo et al. reported such an ordered structure in an aged Fe-30Mn-7.8Al-1.3C alloy, which contains a carbon atom at the body center site, three Fe/Mn atoms randomly at the face center sites, and an Al atom at the corner

TABLE 1 | Room temperature tensile properties of the hot rolled Fe-26Mn-5.84Al-1.0C alloy subjected to various aging treatments.

Methods	AGS (μm)	YS (MPa)	UTS (MPa)	δ_u (%)	δ_f (%)	UTS × δ_f (GPa%)
ST (1,100°C, 1 h)	130	378	764	42.2	47.1	36.0
ST + AT (450°C, 10 h)		375	727	45.1	51.0	37.1
ST + AT (500°C, 10 h)		430	770	49.7	53.2	41.0
ST + AT (550°C, 10 h)		482	898	46.3	50.1	45.0

ST, solution treatment; AT, aging treatment; AGS, average grain size of austenite; YS, yield strength; UTS, ultimate tensile strength; δ_u, uniform elongation; δ_f, elongation to failure.

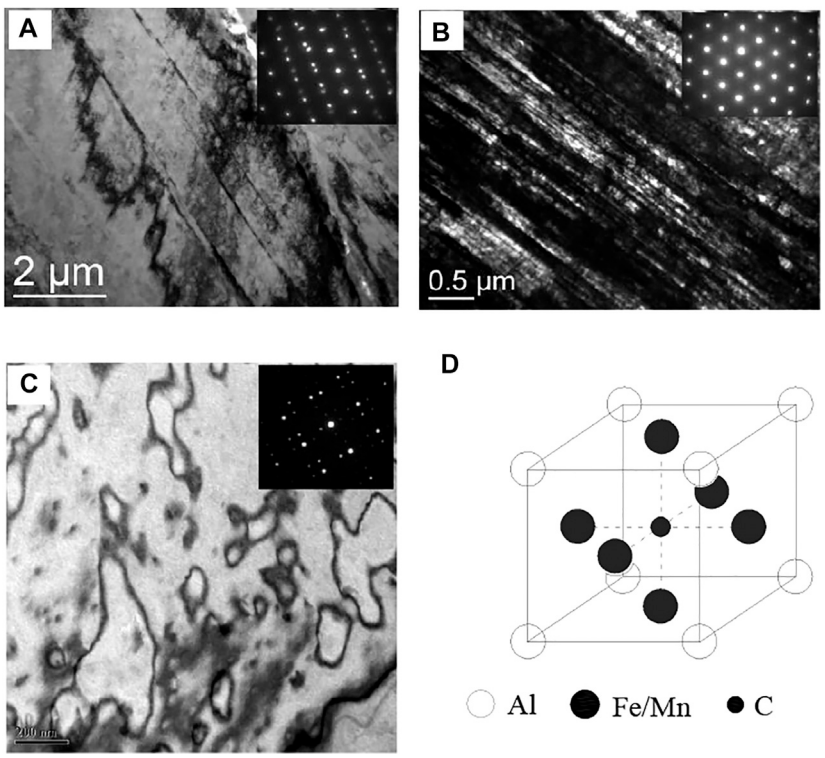

FIGURE 5 | TEM micrographs of Fe-26Mn-5.84Al-1.0C alloy at 550°C for 10 h: **(A)** shows microband and deformation twins as well as the corresponding selected-area diffraction (SAD) patterns; **(B)** shows an ordered island-like phase with a "short-range ordering" (SRO) structure and the corresponding SAD patterns. **(C)** and **(D)** show schematic diagrams of the ordered SRO structure in the Fe-Mn-Al-C quaternary alloy.

positions in its fcc-structured unit cell, as schematically illustrated in **Figure 5D**. The formation of a unit cell of SRO structure involved as follows: Al atom occupies two opposite face centers; Fe and Mn atoms are located on other face centers and each corner; C atom is placed at the center of the unit cell. Because of the ordered arrangement of Al atoms, the SRO patterns of the aged Fe-26Mn-5.84Al-1.0C alloy at 550°C for 10 h were characterized by satellite spots around the fundamental reflections in juxtaposition with superlattice reflections. Furthermore, there existed a certain small tilt angle between the [010] directions of the satellites and fundamental reflections from the [100] superlattice spot. The arrangement of the unit cell in the SRO zone indicates that the short range ordering (SRO) happened after aging treatment at 550°C for 10 h.

The transformation from the γ matrix to SRO caused the formation of short range ordering with an average size of 30–200 nm separated by anti-phase boundaries (APBs). This might be one of the most important factors to obtain the dramatically improved UTS and δ (**Table 1**), owing to the continuously increased strain hardening behavior (**Figure 3**) caused by the precipitation and grain boundary strengthening (**Figure 5**). However, as the Fe-26Mn-5.84Al-1.0C alloy was aged at 550°C for 48 h, the short range ordering disappeared, and the lamellar second-phase precipitates along the grain boundaries were observed in **Figure 6A**. These precipitates were identified as carbide precipitates (Fe, $Mn)_3C_x$ by energy dispersive X-ray spectroscopy (**Figure 6B**), which were also observed previously in Fe-Mn-Al-C alloys (Choo and Han, 1985). Their grain boundary phases were characterized by the ordered κ carbide and a disordered body centered cubic (*bcc*) α ferrite, significantly deteriorating the tensile ductility of Fe-26Mn-5.84Al-1.0C alloy.

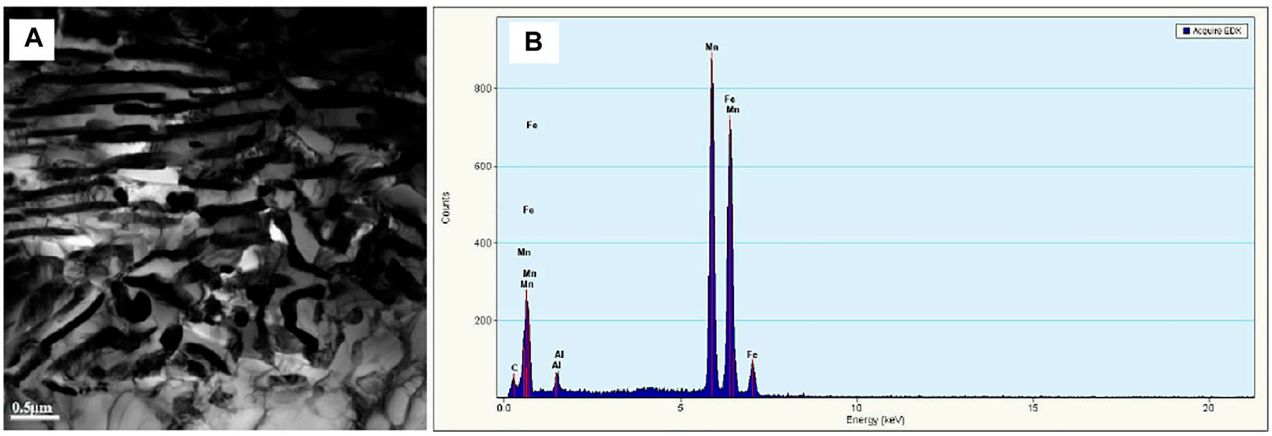

FIGURE 6 | TEM image **(A)** and energy dispersive X-ray spectroscopy (EDS) pattern **(B)** of the aged Fe-26Mn-5.84Al-1.0C alloy at 550°C for 48 h.

CONCLUSION

In summary, a lightweight Fe-26Mn-6Al-1C (mass%) austenitic alloy with a stacking fault energy (SFE) value of approximately 60 mJ·m^{-2} was subjected to solution treatment at 1,100°C for 1 h and various aging treatments at 450–550°C for 10 h. The main conclusions involved as follows:

1) The solution-treated alloy exhibited a relatively large number of dislocations, which were periodically arranged in a plane; whereas an ordered phase with a "short-range ordering" (SRO) structure was observed in the aged sample at 550°C for 10 h. With further increasing aging time to 48 h, the lamellar second-phase precipitates were distributed along grain boundaries.
2) The enhanced ultimate tensile strength (UTS = 898 MPa) and ductility (δ_u = 46.3%) of Fe-26Mn-6Al-1C alloy at 550°C for 10 h was closely associated with relatively high strain hardening in the entire plastic deformation, which was mainly attributed to the formation of an ordered short range ordering.
3) The aged Fe-26Mn-6Al-1C samples at 450–550°C for 10 h exhibited a three-stage strain-hardening behavior and constant strain hardening rate (dσ/dε) at stage II, which was significantly different from the decreased dσ/dε value at stage II for the solution-treated sample.

DATA AVAILABILITY STATEMENT

The original contributions presented in the study are included in the article/Supplementary Material, further inquiries can be directed to the corresponding author.

AUTHOR CONTRIBUTIONS

G-mL: Conceptualization, Methodology, Investigation. HY: Data curation, Writing-Original draft preparation. H-yL: Visualization, Investigation. Y-fJ: Investigation, Supervision. H-tL: Resources, Validation. LK: Formal analysis, Writing-Reviewing and Editing.

FUNDING

This work was financially supported by the National Key R&D Program of China (No. 2018YFB1307902), Open Research Fund from Key Laboratory of Ecological Metallurgy of Multi-metal Intergrown Ores of Ministry of Education (No. NEMM2020003), the Natural Science Foundation of Liaoning Province (No. 2019-KF-25-05), and the Natural Science Foundation of Shanxi Province (No. 201901D111241).

REFERENCES

Choi, K., Seo, C.-H., Lee, H., Kim, S. K., Kwak, J. H., Chin, K. G., Park, K.-T., et al. (2010). Effect of Aging on the Microstructure and Deformation Behavior of Austenite Base Lightweight Fe-28Mn-9Al-0.8C Steel. *Scripta Materialia*. 63, 1028–1031. doi:10.1016/j.scriptamat.2010.07.036

Choi, Y. W., H Dong, Z., Li, W., Schönecker, S., Kim, H., Kwon, S. K., et al. (2020). Predicting the Stacking Fault Energy of Austenitic Fe-Mn-Al (Si) Alloys. *Mater. Des.* 187, 1–8. doi:10.1016/j.matdes.2019.108392

Choo, W. K., and Han, K. H. (1985). Phase Constitution and Lattice Parameter Relationships in Rapidly Solidified (Fe0.65Mn0.35)0.83 Al0.17-xC and Fe3Al-xC Pseudo-binary Alloys. *Metallurgical Transactions A.* 16, 5–10. doi:10.1007/bf02656705

Choo, W. K., Kim, J. H., and Yoon, J. C. (1997). Microstructural Change in Austenitic Fe-30.0wt%Mn-7.8wt%Al-1.3wt%C Initiated by Spinodal Decomposition and its Influence on Mechanical Properties. *Acta Materialia.* 45, 4877–4885. doi:10.1016/s1359-6454(97)00201-2

Ding, H., Li, H. Y., Wu, Z. Q., Huang, M. L., Li, H. Z., and Xin, Q. B. (2013). Microstructural Evolution and Deformation Behaviors of Fe-Mn-Al-C Steels with Different Stacking Fault Energies. *Steel Res. Int.* 84, 1288–1293. doi:10.1002/srin.201300052

Dumay, A., Chateau, J.-P., Allain, S., Migot, S., and Bouaziz, O. (2008). Influence of Addition Elements on the Stacking-Fault Energy and Mechanical Properties of an Austenitic Fe-Mn-C Steel. *Mater. Sci. Eng. A.* 483-484, 184–187. doi:10.1016/j.msea.2006.12.170

Fang, Y., Chen, X., Madigan, B., Cao, H., and Konovalov, S. (2016). Effects of Strain Rate on the Hot Deformation Behavior and Dynamic Recrystallization in China

Low Activation Martensitic Steel. *Fusion Eng. Des.* 103, 21–30. doi:10.1016/j.fusengdes.2015.11.036

Frommeyer, G., and Brüx, U. (2006). Microstructures and Mechanical Properties of High-Strength Fe-Mn-Al-C Light-Weight TRIPLEX Steels. *steel Res. Int.* 77, 627–633. doi:10.1002/srin.200606440

Grassel, O., Frommeyer, G., Derder, C., and Hofmann, H. (1997). Phase Transformations and Mechanical Properties of Fe-Mn-Si-Al TRIP-Steels. *J. Phys. IV* 7, 383–388. doi:10.1051/jp4:1997560

Grässel, O., Krüger, L., Frommeyer, G., and Meyer, L. W. (2000). High Strength Fe-Mn-(Al, Si) TRIP/TWIP Steels Development - Properties - Application. *Int. J. Plasticity*. 16, 1391–1409. doi:10.1016/s0749-6419(00)00015-2

Han, K. H., Yoon, J. C., and Choo, W. K. (1986). TEM Evidence of Modulated Structure in FeMnAlC Austenitic Alloys. *Scripta Metallurgica*. 20, 33–36. doi:10.1016/0036-9748(86)90208-5

Hiraga, K., Hirabayashi, M., Terasaki, O., and Watanabe, D. (1982). One-dimensional Antiphase Structure of Au22Mn6studied by High-Voltage, High-Resolution Electron Microscopy. *Acta Cryst. Sect A.* 38, 269–274. doi:10.1107/s0567739482000576

Huang, Z., Jiang, Y., Hou, A., Wang, P., Shi, Q., Hou, Q., et al. (2017). Rietveld Refinement, Microstructure and High-Temperature Oxidation Characteristics of Low-Density High Manganese Steels. *J. Mater. Sci. Technology*. 33, 1531–1539. doi:10.1016/j.jmst.2017.09.012

Hwang, C. N., Chao, C. Y., and Liu, T. F. (1993). Grain Boundary Precipitation in an Fe-8.0Al-31.5Mn-1.05C alloy. *Scripta Metallurgica et Materialia*. 28, 263–268. doi:10.1016/0956-716x(93)90574-c

Ishida, K., Ohtani, H., Satoh, N., Kainuma, R., and Nishizawa, T. (1990). Phase Equilibria in Fe-Mn-Al-C Alloys. *ISIJ Int.* 30, 680–686. doi:10.2355/isijinternational.30.680

James, P. J. (1969). Precipitation of the Carbide $(Fe,Mn)_3AlC$ in an Fe-Al Alloy. *J. Iron Steel Inst.* 207, 54–57.

Kalashnikov, I., Acselrad, O., Shalkevich, A., and Pereira, L. C. (2000). Chemical Composition Optimization for Austenitic Steels of the Fe-Mn-Al-C System. *J. Mater. Eng. Perform.* 9, 597–602. doi:10.1361/105994900770345430

Kayak, G. L. (1969). Fe-Mn-Al Precipitation-Hardening Austenitic Alloys. *Met. Sci. Heat Treat.* 11, 95–97. doi:10.1007/bf00652271

Klimova, M., Zherebtsov, S., Stepanov, N., Salishchev, G., Haase, C., and Molodov, D. A. (2017). Microstructure and Texture Evolution of a High Manganese TWIP Steel during Cryo-Rolling. *Mater. Characterization*. 132, 20–30. doi:10.1016/j.matchar.2017.07.043

Li, K.-w., Zhuang, C.-l., Liu, J.-h., Shen, S.-b., Ji, Y.-l., and Han, Z.-b. (2015). Smelting and Casting Technologies of Fe-25Mn-3Al-3Si Twinning Induced Plasticity Steel for Automobiles. *J. Iron Steel Res. Int.* 22, 75–79. doi:10.1016/s1006-706x(15)30142-4

Li, Z., Wang, Y. C., Cheng, X. W., Liang, J. X., and Li, S. K. (2020). Compressive Behavior of a Fe-Mn-Al-C Lightweight Steel at Different Strain Rates. *Mater. Sci. Eng. A.* 772, 1–9. doi:10.1016/j.msea.2019.138700

Luo, Z. C., and Huang, M. X. (2018). Revisit the Role of Deformation Twins on the Work-Hardening Behaviour of Twinning-Induced Plasticity Steels. *Scripta Materialia*. 142, 28–31. doi:10.1016/j.scriptamat.2017.08.017

Sarkar, A., Sanyal, S., Bandyopadhyay, T. K., and Mandal, S. (2019). Implications of Microstructure, Taylor Factor Distribution and Texture on Tensile Properties in a Ti-Added Fe-Mn-Al-Si-C Steel. *Mater. Sci. Eng. A.* 767, 1–12. doi:10.1016/j.msea.2019.138402

Sohn, S. S., Lee, S., Lee, B.-J., and Kwak, J.-H. (2014). Microstructural Developments and Tensile Properties of Lean Fe-Mn-Al-C Lightweight Steels. *JOM*. 66, 1857–1867. doi:10.1007/s11837-014-1128-3

Song, R., Cai, C., Liu, S., Feng, Y., and Pei, Z. (2017). Stacking Fault Energy and Compression Deformation Behavior of Ultra-high Manganese Steel. *Proced. Eng.* 207, 1809–1814. doi:10.1016/j.proeng.2017.10.943

Urrutia, I. G., and Raabe, D. (2011). Dislocation and Twin Substructure Evolution During Strain Hardening of an Fe-22 wt.% Mn-0.6 wt.% C TWIP Steel Observed by Electron Channeling Contrast Imaging. *Acta Mater.* 59, 6449–6462. doi:10.1016/j.actamat.2011.07.009

Yuan, X., Chen, L., Zhao, Y., Di, H., and Zhu, F. (2015). Influence of Annealing Temperature on Mechanical Properties and Microstructures of a High Manganese Austenitic Steel. *J. Mater. Process. Technology* 217, 278–285. doi:10.1016/j.jmatprotec.2014.11.027

Conflict of Interest: The authors declare that the research was conducted in the absence of any commercial or financial relationships that could be construed as a potential conflict of interest.